Advanced Powder Technology 28 (2017) 223–229

Contents lists available at ScienceDirect

Advanced Powder Technology

journal homepage: www.elsevier.com/locate/apt

Original Research Paper

Solid state amorphization of Mg-Zn-Ca system via mechanical alloying and characterization

Bhaskar Manne [a], Srikanth Bontha [b], M.R. Ramesh [b,*], Munishamaiah Krishna [c], Vamsi Krishna Balla [d]

[a] Department of Mechanical Engineering, CMR Institute of Technology, Bengaluru 560037, India
[b] Department of Mechanical Engineering, National Institute of Technology Karnataka, Surathkal, Mangalore 575025, India
[c] Department of Mechanical Engineering, R.V. College of Engineering, Bengaluru 560059, India
[d] Bioceramics and Coating Division, CSIR-Cental Glass and Ceramic Research Institute, Kolkata 700032, India

ARTICLE INFO

Article history:
Received 15 March 2016
Received in revised form 19 September 2016
Accepted 27 September 2016
Available online 22 October 2016

Keywords:
Solid state reaction
Mechanical alloying
Amorphization
X-ray diffraction (XRD)
Thermal analysis

ABSTRACT

Magnesium based bulk metallic glasses have attracted significant attention of researchers due to better mechanical and corrosion properties when compared to their crystalline counterparts especially for biomedical applications. Scaling up the part size and production volumes of such materials through liquid metallurgy route is challenging. In this work amorphous $Ca_5Mg_{60+X}Zn_{35-x}$ (X = 0, 3 and 7) alloys have been successfully synthesized through solid state amorphization using a high energy planetary ball mill. X-ray diffraction was used to identify the crystalline phases of the powder during reaction. Evolution of amorphous phase was analysed using a parameter involving the ratio of integral area of peaks to the integral area of background (I_{PB}) obtained from XRD patterns. Results showed reaction time increases with decreasing Zn content in $Ca_5Mg_{60+X}Zn_{35-x}$ (X = 0, 3 and 7) alloy to obtain maximum amorphous structure with a small amount of residual crystalline phase. Prolonged milling of these powders, to eliminate residual crystalline phases, resulted in the nucleation of $Mg_{102.08}Zn_{39.6}$ phase. The composition dependent characteristic temperatures and thermal stabilities were studied using differential scanning calorimetry.

1. Introduction

Magnesium based materials have attracted the interest of many researchers for biomedical applications due to their physical, mechanical and biodegradable properties. However, the high rate of biodegradation and hydrogen evolution are the major problems of Mg based alloys especially for biomedical applications [1]. Degradation or corrosion is a surface phenomenon in Mg alloys and the penetration of corrosive products into the alloy depends on the type of secondary phases and their distribution. The network of secondary phases present at the grain boundaries accelerate galvanic corrosion of adjacent matrix and promote stress corrosion [2]. Currently researched Mg-Zn-Ca based bulk metallic glasses (BMG) have shown decreased degradation rates due to the absence of grain boundaries and chemical homogeneity. They also, exhibit high strength and ductility [3,4]. The part dimensions of these BMG's produced by copper mold casting technique are limited to a few millimetres and close control of composition is difficult due to elemental evaporation. Further, rapid solidification techniques require complex environment for processing as all the three elements (Mg, Zn and Ca) are highly reactive with oxygen and moisture. Mechanical alloying by high energy ball milling techniques can potentially surpass the difficulties associated with processing BMG's using conventional methods. Further, the synthesized powders can be consolidated to full density in desired shapes using both conventional routes, such as cold pressing and sintering, and non-conventional routes like plasma arc sintering, pulsed current sintering and 3D laser printing.

Calka et al. in 1989 produced the first Mg-Zn amorphous alloy by ball milling of prealloyed powders. Their study reported that mechanically alloyed powders exhibited lower thermal stability compared to melt spun method and exothermic peak in DSC traces corresponds to crystallization was broad over a range of temperature [5]. Later syntheses of amorphous phase through mechanical alloying and consolidation techniques have been explained in the literature for Mg-Y-Cu system [6,7] and Mg-Ni-Si systems [8]. A major interest was showed on Mg-Zn-Ca system for biomedical applications due to the involvement of these elements in the human metabolism and products of corrosion

* Corresponding author.
E-mail address: rameshmr@nitk.edu.in (M.R. Ramesh).

http://dx.doi.org/10.1016/j.apt.2016.09.032
0921-8831/

can be excreted out of the body safely for maintaining the balanced human metabolism. Also, another functional application of this class of materials is azo dyes (potential organic pollutants in water) degradation. Wang et al. [9] synthesized Mg-Zn-Ca based amorphous powders via melt quenching of the master alloy on a rotating copper wheel to produce amorphous ribbons. Ball milling was then carried out to decrease the particle size. Their work explored this class of material for degrading azo dyes. They reported that the azo dyes degrading ability of this class of materials is 1000 times greater than the commercially available Fe based crystalline materials and around 20 times greater than Mg based crystalline materials. Zhao et al. [10] used the gas atomization technique to produce Mg-Zn-Ca amorphous powders. Their study also reported excellent azo dyes degrading ability of the Mg-Zn-Ca system. Even though high production volumes can be synthesized using the gas atomization technique, the environmental conditions required for processing are complex. Datta et al. [11] studied the application of Mg-Zn-Ca alloy for biomedical implants. In this work, a nominal composition of $Mg_{60}Zn_{35}Ca_5$ amorphous powder was synthesized using the SPEX 8000 shaker ball mill. Although the shaker mills are known for their short reaction times, the number of milling batches and associated man hours are high for the production of large volumes of powders. Also, the order of particle size which was obtained through shaker mills in the above study is highly difficult to handle in the atmospheric conditions while consolidating into a product (This problem is also observed in the present work when the particle size reduced to below 0.5 μm). High energy planetary ball mills are known for high production volumes per batch as compared to shaker mills [12]. Therefore, in this work the potentiality of solid state amorphization of $Ca_5Mg_{60+x}Zn_{35-x}$ ($X = 0$, 3 and 7) is explored using a high energy planetary ball mill. X-ray diffraction (XRD) studies are performed to examine the progress of reaction in the ball milling process. Differential scanning calorimetry (DSC) studies are used to understand the crystallization characteristics in the milled powders.

2. Experimental procedures

2.1. Synthesis of amorphous powders

Elemental powders of Mg (99.8%, −325 mesh), Zn (99.9%, −100 mesh) and Ca (99%, −6 mesh) were precisely measured to yield desired composition of $Ca_5Mg_{60+x}Zn_{35-x}$ ($X = 0$, 3 and 7) alloy. The elemental powders were subjected to mechanical alloying in a Fretsch (Pulverisette 6) planetary ball mill. This planetary mono mill has a disc speed of 650 rpm and is programmable for both cycle time and reversing cycles. Milling was carried out with a ball to powder (BPR) weight ratio of 10:1 in a sealed stainless steel vial using 10 mm stainless steel balls. Loading, scrapping of the powders stuck to the vial, sampling and batching of powders were carried out in a glove box with an argon atmosphere. Milling was performed at a speed between 250 and 300 rpm to avoid excessive heating and consequent crystallization of synthesized alloy. Ten minutes of idle time after every thirty minutes of milling was programmed to avoid excessive heating of the vial. Reversed milling was used after each cycle of milling. A total of carefully weighed 30 g of powders were added to the vial for the reaction. Initially milling of Ca was carried out, in 0.3 ml/g of toluene, to reduce the particle size and enhance the diffusion as its particle size was relatively larger than that of Mg and Zn. Later, Mg and Zn were added to the vial along with 3–4% of toluene as a process control agent. To avoid adhesion of the powders to the vial, 1 ml of toluene was added after eight hours for every eight to ten cycles of milling.

2.2. Characterization

The process of amorphization was examined by X-ray diffraction (XRD) analysis of a small amount of mechanically alloyed samples collected at different intervals of milling. The XRD patterns were obtained by Rigaku Miniflex II equipped with Cu Kα monochromator (1.5406 Å), operating at 40 kV and 30 mA. The scanning range was 10–80° with a scan speed of 2°/min and step size of 0.01°. The analysis of the X-ray pattern was carried out using X'pert HighScore Plus Rietveld analysis software loaded with ICDD database PDF-2.

In the process of solid state amorphization, the intensity of amorphous background grows as a function of milling time while the intensity of crystalline peaks decreases. Therefore, the ratio of integral area of peaks to integral area of the background was used as a parameter to analyse the advancement of the reaction in ball milling and it is mathematically expressed as

$$I_{PB} = I_P / I_B \tag{1}$$

where I_{PB} is a ratio of integral area of peaks (I_P) to integral area of background (I_B). The ratio and slope tend to infinity when the material is crystalline and tend to zero when the material is completely amorphous.

The X'pert High Score software was used to extract the background intensities from the diffraction pattern which runs with an automatic mode and approximates the background iteratively according to Sonneveld et al. [13]. The adjustable parameters in this mode were granularity and bending factor. Granularity influences the number of intervals used for determining the background while bending factor influences the curvature effects. In this work, the granularity was set to 5% and bending factor to 0% (in order to avoid curvature effects near the diffraction peaks) for all the analysis. Integral area of the background (extracted from X'pert HighScore software) and integral area of the total diffraction was calculated using OriginPro 8.0 software. The integral area of the peaks is the difference of integral area of the total diffraction and the integral area of the background. In order to compute integral area under background, the intensity of the background with respect to diffraction angles is extracted using X'pert HighScore software by adjusting the mentioned parameters. An illustration of extraction of background intensities is shown in Fig. 1.

The morphology and size of the particles was studied using JEOL JSM-6380LA scanning electron microscope (SEM). Thermal analysis was carried out to estimate the apparent activation energies needed to understand the thermal stability using Perkin Elmer differential scanning calorimeter (DSC) operated under the continuous flow of nitrogen gas. The DSC traces were obtained in the temperature range of 30–450 °C. The characteristic temperatures were determined by taking an average of 3 DSC traces on each sample.

3. Results and discussions

3.1. Solid state amorphization

Fig. 2 shows particle morphology changes during milling and Fig. 3 shows the morphology of the milled powders. It is evident from Fig. 2 that particle flattening, cold welding, plastic deformation of welded particles and fracturing are continuous phenomenon in scaling down the particles in mechanical alloying. In the process of mechanical alloying, interdiffusion of atoms in the welded layers dominates the self diffusion in the elements. This is because of the high impact energy and microscopic temperatures generated in milling. The occurrence of interdiffusion can also be supported by the large negative heat of mixing of the elements. Later the formation and stability of amorphous or

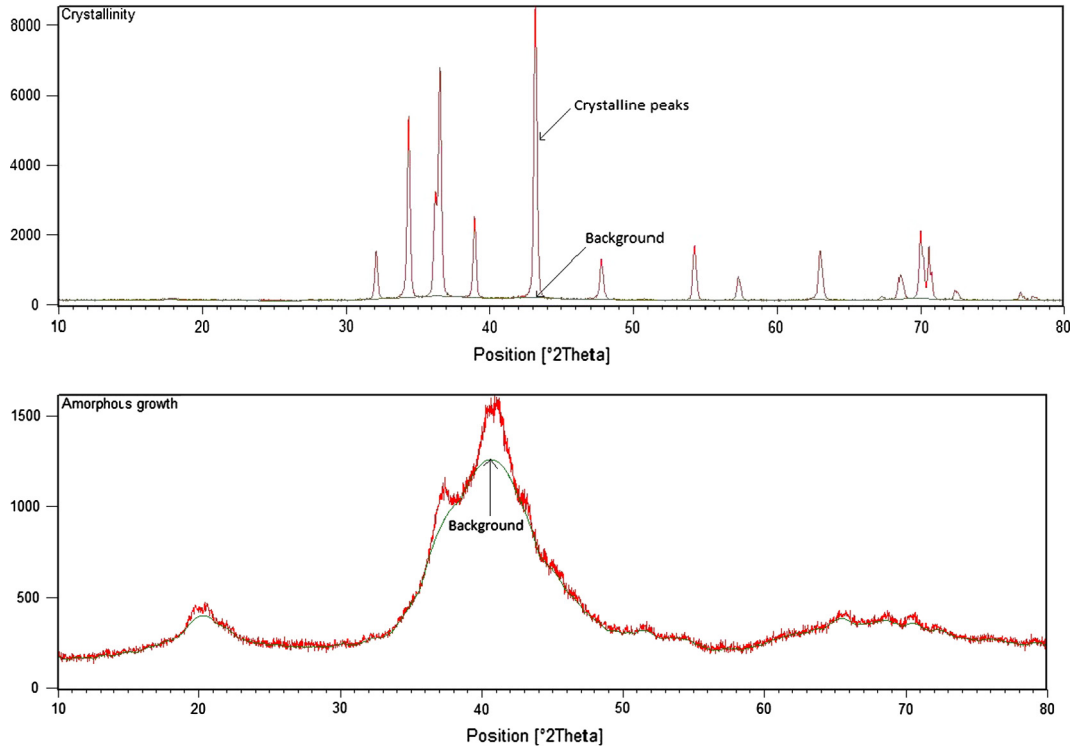

Fig. 1. Illustration of extraction of background and crystalline peak intensities for I_{PB} calculations.

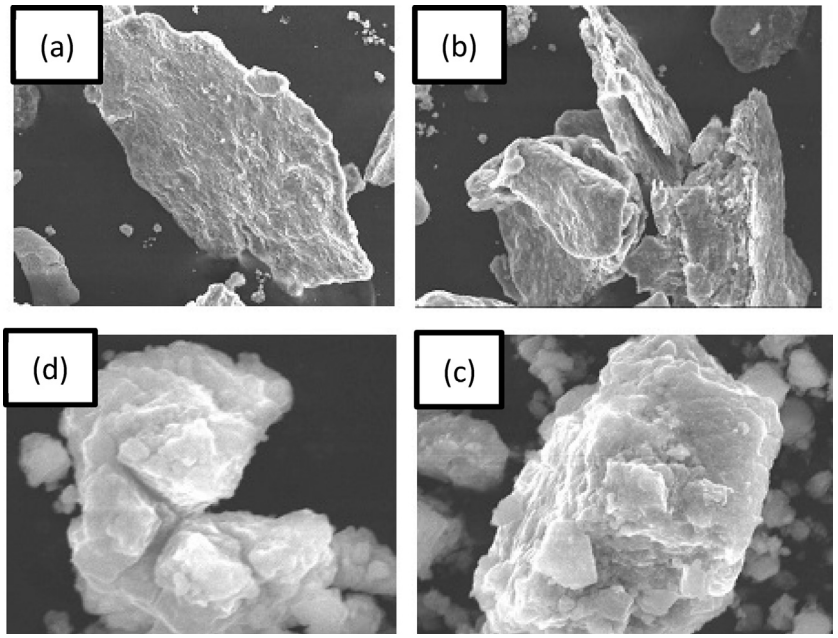

Fig. 2. SEM micrographs showing particle morphology during milling: (a) flattening, (b) cold welding, (c) plastic deformation and (d) fracturing.

non-equilibrium crystalline phase depends on whichever the phase has lowest free energy state. The final morphology of the milled powders, shown in Fig. 3, was of non-layered structure and the particle sizes were 0.9–1.1 μm, 1.5–2.2 μm and 2–2.5 μm for $X = 0$, 3 and 7 respectively in $Ca_5Mg_{60+x}Zn_{35-x}$ after milling. It appears that the particle size decreases with increase in the concentration of Zn in the alloy. The variation in the particle size could be attributed to different amounts of plastic deformation and fracturing for varied compositions. Generally, the strength/hardness of Mg-Zn alloy increases with increase in the Zn concentration [14] enabling better fragmentation of the alloy powder during milling. On the other hand, when the alloy contain high amount of Mg, i.e., low concentration of Zn, the ductility of the system will be high and therefore particle fragmentation become difficult. Therefore, in general the particle size decreased with increase in the Zn concentration of present alloy.

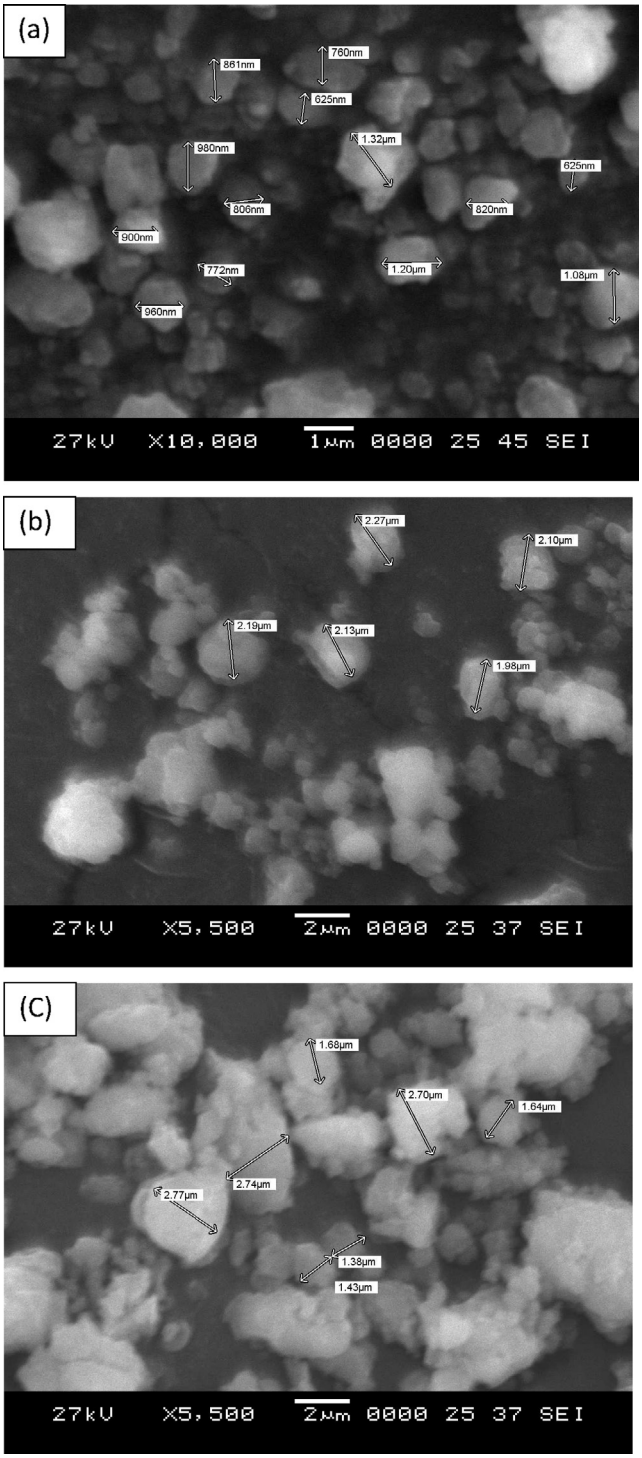

Fig. 3. SEM micrographs showing morphology and size of mechanically alloyed powders: (a) $X = 0$ (20 h), (b) $X = 3$ (21 h) and (c) $X = 7$ (21.5 h) in $Ca_5Mg_{60+x}Zn_{35-x}$.

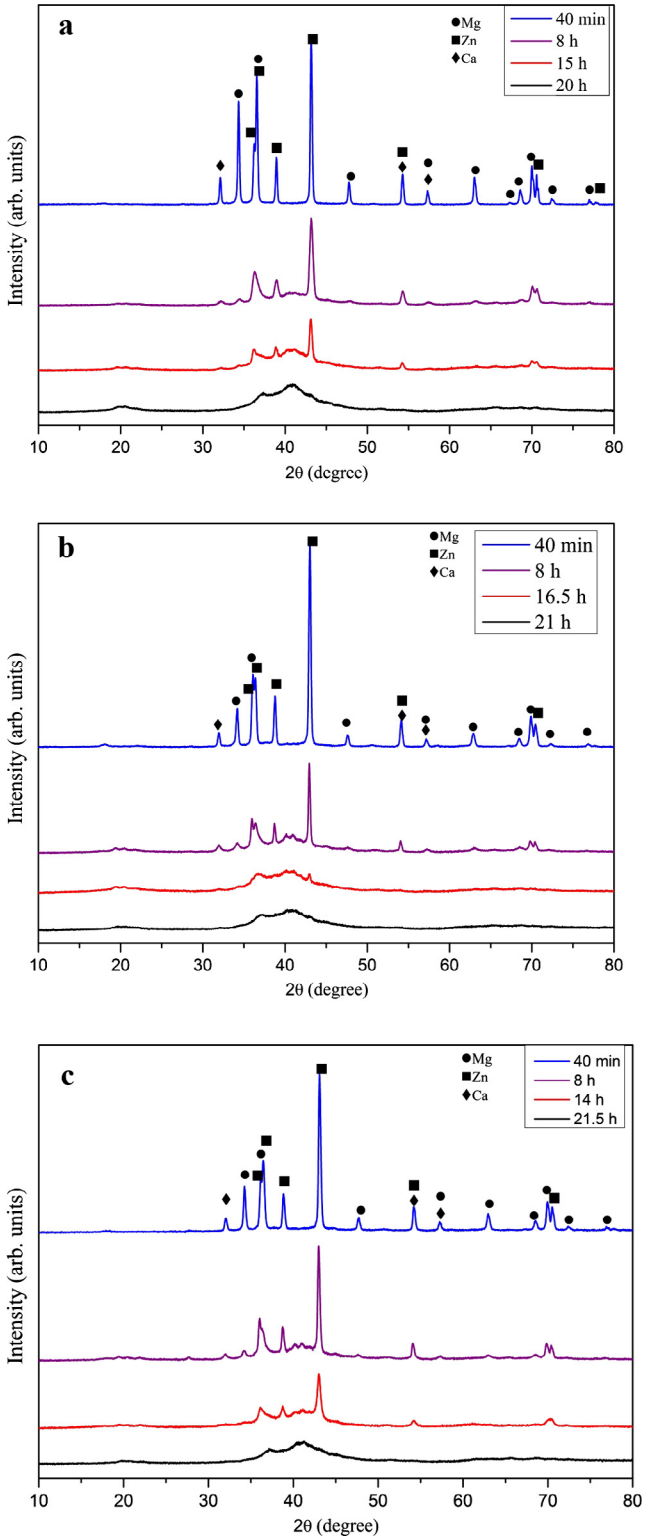

Fig. 4. XRD patterns of milled $Ca_5Mg_{60+x}Zn_{35-x}$ where (a) $X = 0$ (b) $X = 3$ and (c) $X = 7$ at various time durations.

XRD patterns obtained at various intervals of milling are presented in Fig. 4. Continuous decrease in the intensity and broadening of the native crystalline peaks was observed as a function of milling time. No peaks correspond to any intermetallics was noticed from XRD peaks during the course of reaction. The initiation of amorphization (characteristics amorphous background) can be clearly seen after 8 h of milling in all three compositions. The amorphous phase gradually became dominant after 14–15 h of milling. The formation of amorphous hallo hump was observed at $2\theta = 22°$, 35–45° and 55–75°. The reaction times were observed to be 20 h, 21 h and 21.5 h for $X = 0$, 3 and 7, respectively, in $Ca_5Mg_{60+x}Zn_{35-x}$ composition to obtain amorphous structure with a small amount of residual crystalline phase. The reaction trends studied with I_{PB} as a function of milling time are shown in Fig. 5. The value of I_{PB} provides a qualitative index of amorphization,

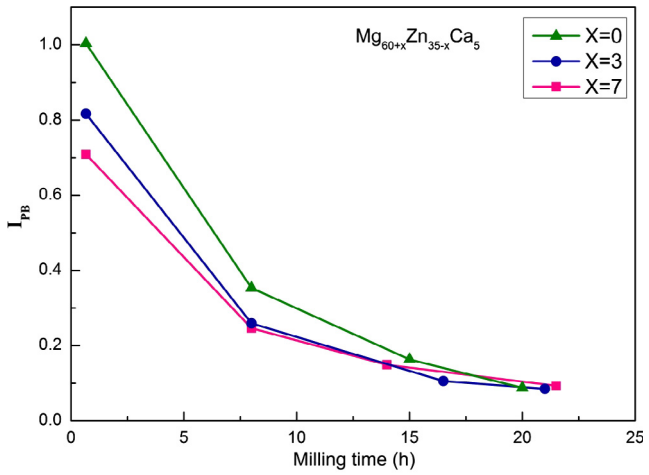

Fig. 5. Illustration of change in integral area of peak to background ratio with the variation of milling time and composition.

which varies generally from one (crystalline) to zero (amorphous). Initial I_{PB} value of the alloys containing higher Zn concentration was found to be high and decreased with decreasing Zn concentration. This may be due to dominant un-diffused Zn crystalline phase over amorphous phase in the alloys with high concentration of Zn. The general trends showed negative slope moving from higher slopes at the beginning of the reaction tending towards zero slope at the end of the reaction. These trends indicate change of crystalline phase to amorphous phase in the alloys as a function of milling time. Increased slope and reduced reaction time was noticed with the increase in Zn loading. This can be attributed to increase in crystal straining caused by Zn alloying. The value of I_{PB} was found to be 0.08, 0.12 and 0.10 for $X = 0$, 3 and 7 respectively in $Ca_5Mg_{60+x}Zn_{35-x}$ at the end of the reaction. This is because of the small residual crystalline peak retained in these alloys. Several researchers have observed a broad hallow peak in these compositions with different amorphization techniques without any residue [12,15,16]. However, the small amount of residue retained in the hallow peak could not be avoided in the present work. Further, prolonged milling of the powders resulted in the nucleation of $Mg_{102.08}Zn_{39.6}$ phase and small traces of MgZn intermetallic nanophases from the amorphous phase (Fig. 6). The nucleation of such phases was even noticed in the isothermal heat treatment of $Ca_5Mg_{67}Zn_{28}$ amorphous ribbons above the temperature of 160 °C [17]. The microscopic temperatures in milling were reported to be very high even though the temperature of the vial is at room temperatures [12]. Also, the availability of large surface area of the scaled down particles in the milling process could enhance the heat transfer to the particle. These could be the reasons for the in-situ heat treatment and nucleation of new phases in the course of prolonged milling. Similar nucleation of new phases from amorphous phase was also observed in other ternary systems by the mechanical alloying route [18,19].

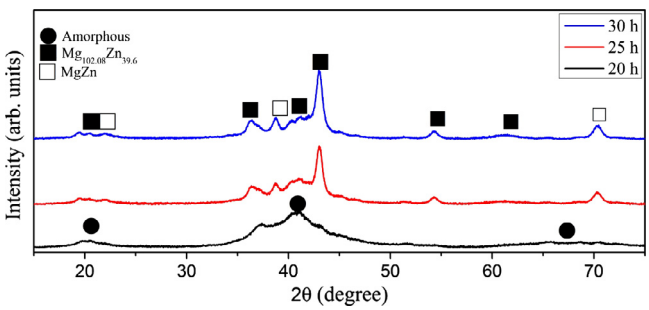

Fig. 6. XRD patterns illustrating nano-crystallization from amorphous phase in $Ca_5Mg_{60}Zn_{35}$ alloy during milling.

3.2. Characteristic temperatures and thermal stability

Fig. 7 shows the DSC traces of synthesized powders (I_{PB} = 0.78, 0.13 and 0.11 for $X = 0$, 3 and 7 respectively with the range of particle size mentioned in Section 3.1) obtained at a constant heating rate of 40 K/min. Traces showed start of crystallization temperature (T_x), peak exothermic temperatures (T_{p1} and T_{p2}) which correspond to peak crystallization events and an endothermic event (T_l) may corresponds to solid state transformation or melting of phases. Composition dependent characteristic temperatures extracted from DSC traces are shown in Fig. 8. The variation of these characteristic temperatures obtained from DSC traces was ±2 °C. All the characteristic temperatures monotonically increased with the increase in Zn alloying content in $Ca_5Mg_{60+x}Zn_{35-x}$. Start of crystallization (T_x) events and first peak crystallization events were found to be increased for $x = 0$, 3 and 7 respectively. Second peak crystallization was observed for the two compositions $Ca_5Mg_{67}Zn_{28}$ and $Ca_5Mg_{63}Zn_{32}$ while the $Ca_5Mg_{60}Zn_{35}$ did not show the same. Endothermic events were observed at around 627 K in all the DSC traces of the compositions studied. Another endothermic event was observed for $Ca_5Mg_{60}Zn_{35}$.

In order to understand the dependency of crystallization events with the heating rates, DSC studies were carried out at different heating rates. The DSC traces of one powder composition $Ca_5Mg_{67}Zn_{28}$ at heating rates of 10 K/min, 15 K/min, 20 K/min, 40 K/min and 60 K/min is depicted in Fig. 9. It is clear from these traces that, peak crystallization temperatures (T_{p1} and T_{p2}) shift to higher values with increase in the heating rate indicating that the nucleation and phase transformations are thermal activated processes. The apparent activation energies were estimated for the first peak crystallization event (T_{p1}) using Kissinger's method [20]. This calculation is based on sensitivity (shifting to higher values) of characteristic temperatures to the heating rates and is given as.

$$\ln(T^2/\beta) = E/RT + C \quad (2)$$

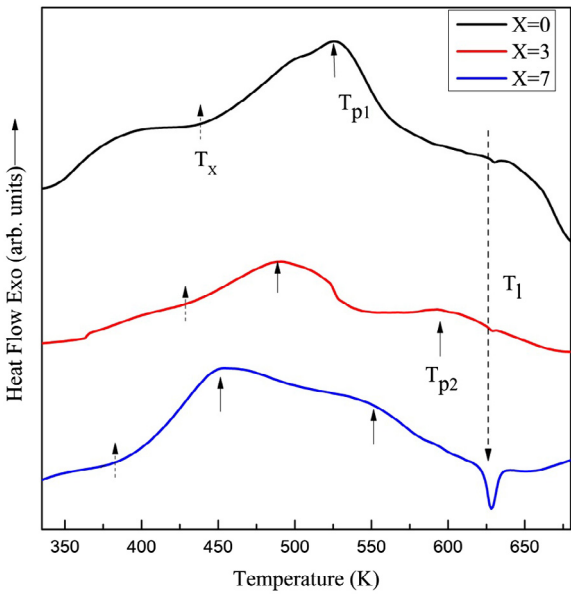

Fig. 7. DSC traces of mechanically alloyed $Ca_5Mg_{60+x}Zn_{35-x}$ ($X = 0$–7) taken at 40 K/min heating rate.

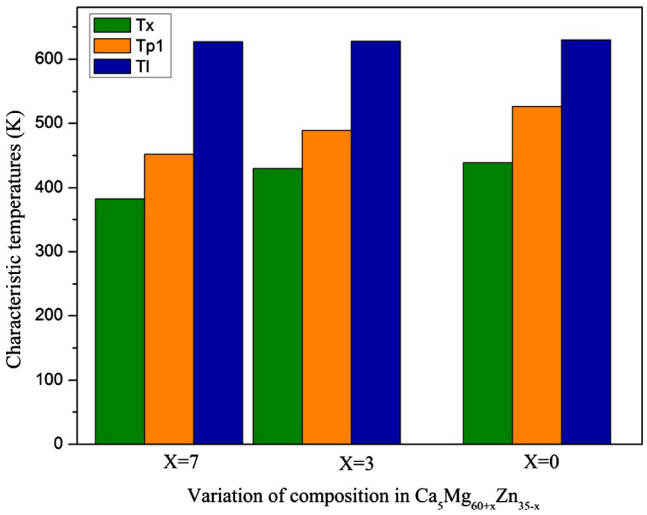

Fig. 8. Composition dependent characteristic temperatures for milled $Ca_5Mg_{60+x}Zn_{35-x}$ ($X = 0$, 3 and 7).

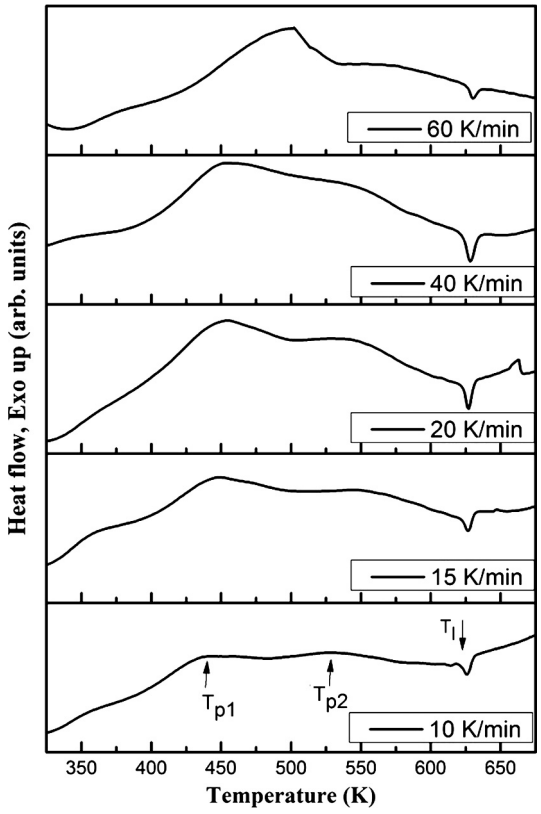

Fig. 9. DSC traces of milled $Ca_5Mg_{67}Zn_{28}$ powder at heating rates of 10 K/min, 15 K/min, 20 K/min, 40 K/min and 60 K/min.

where E is the apparent activation energy, T is the characteristic temperature, β is the heating rate and R is the gas constant. The slope of plot $\ln(T^2/\beta)$ versus $1/RT$ gives the associated apparent activation energy for the given characteristic temperature. The Kissinger's plot for the first peak crystallization event T_{p1} of the composition $Ca_5Mg_{60+x}Zn_{35-x}$ ($X = 0$, 3 and 7) is shown in Fig. 10. The activation energies thus estimated were found to be 144.84 kJ/mole, 52.108 kJ/mole and 44.95 kJ/mole for $x = 0$, 3 and 7, respectively. These activation energies were observed to be much lower in order as compared to the alloys synthesized through liquid metallurgy

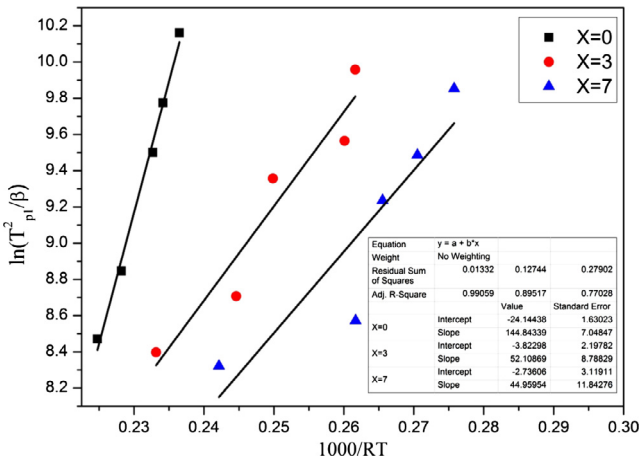

Fig. 10. Kissinger's plot for milled $Ca_5Mg_{60+x}Zn_{35-x}$ ($X = 0$, 3 and 7).

route [21,22]. This is due to the known fact that mechanically alloyed compositions exhibit layered structure and the alloying of the innermost layers cannot be ensured. Thermal stability of the amorphous alloys were found to be more sensitive to Mg concentrations and decreased with the increase in the Mg concentration in contrary to that reported in literature [21,22]. This variation could be attributed to the residual crystallinity retained in amorphous phase synthesized. The crystallinity present in the amorphous phase acts as a nucleus for further crystalline growth in the material under thermal activation. This results in a reduction in the thermal stability of the material which can be observed as a shift in the characteristic temperatures in the DSC traces [23,24].

4. Conclusions

Amorphous $Ca_5Mg_{60+x}Zn_{35-x}$ ($X = 0$, 3 and 7) alloys were synthesized using high energy planetary ball milling and the conclusions from the work are outlined as below.

1. High energy planetary ball milling method by passed the potential environmental risks of bulk amorphous alloy production via liquid metallurgy route with high production volumes of powder viable for mass production of parts for biomedical, structural and degrading azo dyes in water treatment applications. Critically resulted particle sizes in ball milling of 1–2.5 μm were sufficient to bypass powder handling problems in air for consolidation into parts without any flames.
2. Reaction times of milling and particle size were found to be composition dependent.
3. Prolonged milling to avoid native crystalline peaks and to obtain completely amorphous phase had resulted in the nucleation of $Mg_{102.08}Zn_{39.6}$ and along with the traces of MgZn nanophases.
4. The quality of amorphous phase was assessed by a parameter involving ratio of integral area of peaks to integral area of background (I_{PB}) obtained from XRD pattern. These trends were found to be composition dependent.
5. The thermal stabilities of the alloys were evaluated using Kissinger's plot taking the peak crystallization temperatures from the DSC traces. Results reveal that the thermal stability of these alloys was found to be lower than alloys synthesized conventionally through liquid metallurgy route.
6. This work provides future scope for consolidation of the alloyed powders to a bulk component. The mechanical properties and corrosion behaviour can be evaluated for biomedical and structural applications. These powders can also be explored for azo dyes degrading in pollute water.

References

[1] F. Witte, The history of biodegradable magnesium implants: a review, Acta Biomater. 6 (2010) 1680–1692.
[2] A. Atrens, M. Liu, N. Ishide, Z.A. Bidin, Corrosion mechanism applicable to biodegradable magnesium implants-review, Mater. Sci. Eng., B 176 (2011) 1609–1636.
[3] X. Gu, G.J. Shilet, F.Q. Guoa, S.J. Poona, Mg–Ca–Zn bulk metallic glasses with high strength and significant ductility, J. Mater. Res. 20 (2005) 1935–1938.
[4] B. Zberg, P.J. Uggowitzer, J.F. Löffler, MgZnCa glasses without clinically observable hydrogen evolution for biodegradable implants, Nat. Mater. 8 (2009) 887–890.
[5] A. Calka, A.P. Radlinski, Amorphization of Mg–Zn alloys by mechanical alloying, Mater. Sci. Eng., A 118 (1989) 131–135.
[6] P.Y. Lee, M.C. Kao, C.K. Lin, J.C. Huang, Mg–Y–Cu bulk metallic glass prepared by mechanical alloying and vacuum hot-pressing, Intermetallics 14 (2006) 994–999.
[7] P.Y. Lee, C. Lo, J.S.C. Jang, Consolidation of mechanically alloyed $Mg_{49}Y_{15}Cu_{36}$ powders by vacuum hot pressing, J. Alloys Compd. 434–435 (2007) 354–357.
[8] K. Ozaki, T. Nishio, A. Matsumoto, K. Kobayashi, Preparing Mg–Ni–Si amorphous powders by mechanical alloying and consolidation by pulsed current sintering, Mater. Sci. Eng., A 375–377 (2004) 857–860.
[9] J.-Q. Wang, Y.-H. Liu, M.-W. Chen, D.V. Louzguine-Luzgin, A. Inoue, J.H. Perepezko, Excellent capability in degrading azo dyes by MgZn-based metallic glass powders, Sci. Rep. 2 (2012) 1–6.
[10] Y.F. Zhao, J.J. Si, J.G. Song, Q. Yang, X.D. Hui, Synthesis of Mg–Zn–Ca metallic glasses by gas-atomization and their excellent capability in degrading azo dyes, Mater. Sci. Eng., B 181 (2014) 46–55.
[11] M.K. Datta, D.-T. Chou, D. Hong, P. Saha, S.J. Chung, B. Lee, A. Sirinterlikci, M. Ramanathan, A. Roy, P.N. Kumta, Structure and thermal stability of biodegradable Mg–Zn–Ca based amorphous alloys synthesized by mechanical alloying, Mater. Sci. Eng., B 176 (2011) 1637–1643.
[12] C. Suryanarayana, Mechanical alloying and milling, Prog. Mater. Sci. 6 (2001) 1–184.
[13] E.J. Sonneveld, J.W. Visser, Automatic collection of powder data from photographs, J. Appl. Cryst. 8 (1975) 1–7.
[14] E. Koç, M.B. Kannan, M. Ünal, E. Candan, Influence of zinc on the microstructure, mechanical properties and in vitro corrosion behavior of magnesium–zinc binary alloys, J. Alloys Compd. 648 (2015) 291–296.
[15] B. Zberg, E.R. Arata, P.J. Uggowitzer, J.F. Löffler, Tensile properties of glassy MgZnCa wires and reliability analysis using Weibull statistics, Acta Mater. 57 (2009) 3223–3231.
[16] Y.-Y. Zhao, E. Ma, J. Xu, Reliability of compressive fracture of Mg-Zn-Ca bulk metallic glasses: flaw sensitivity and Weibull statistics, Scr. Mater. 58 (2008) 496–499.
[17] Y. Wang, M.J. Tan, J. Pang, Z. Wang, A.W.E. Jarfors, In vitro corrosion behaviors of $Mg_{67}Zn_{28}Ca_5$ alloy: from amorphous to crystalline, Mater. Chem. Phys. 134 (2012) 1079–1087.
[18] P. Nidhi, P.M.G. Nambissan, I. Manna, Amorphisation and intermetallic nanophase formation in ball-milled Al-Ti-Si studied through positron lifetime spectroscopy, J. Alloys Compd. 377 (2004) 179–187.
[19] S. Kanchibhotla, N. Munroe, T. Kartikeyan, Amorphization in Ni-Ti-Ta system through mechanical alloying, J. Mater. Sci. 40 (2005) 5003–5006.
[20] H.E. Kissinger, Reaction kinetics and differential thermal analysis, Anal. Chem. 29 (1957) 1702–1706.
[21] Y.E. Zhang, G.J. Rocher, B. Briccoli, D. Kevorkov, X.B. Liu, Z. Altounian, M. Medraj, Crystallization characteristics of the Mg-rich metallic glasses in the Ca–Mg–Zn System, J. Alloys Compd. 552 (2013) 88–97.
[22] Y.F. Zhao, J.J. Si, J.G. Song, Q. Yang, X.D. Hui, Synthesis of Mg–Zn–Ca metallic glasses by gas-atomization and their excellent capability in degrading azo dyes, Mater. Sci. Eng., B 181 (2014) 46–55.
[23] M. Ramya, S.G. Sarwat, V. Udhayabanu, S. Subramanian, B. Raj, K.R. Ravi, Role of partially amorphous structure and alloying elements on the corrosion behavior of Mg–Zn–Ca bulk metallic glass for biomedical applications, Mater. Des. 86 (2015) 829–835.
[24] V.K. Balla, A. Bandyopadhyay, Laser processing of Fe-based bulk amorphous alloy, Surf. Coat. Technol. 205 (2010) 2661–2667.